J|A|C|S
ARTICLES
Published on Web 12/13/2003

Hexakis(4-iodophenyl)-*peri*-hexabenzocoronene- A Versatile Building Block for Highly Ordered Discotic Liquid Crystalline Materials

Jishan Wu, Mark D. Watson,*,† Li Zhang, Zhaohui Wang, and Klaus Müllen*,†

Contribution from the Max-Planck Institute for Polymer Research, Ackermannweg 10, D-55128, Mainz, Germany

Received July 24, 2003; E-mail: muellen@mpip-mainz.mpg.de

Abstract: Hexakis (4-iodophenyl)-*peri*-hexabenzocoronene (**5**), a novel functionalizable mesogenic building block, was prepared by rational multistep synthesis. Although sparingly soluble in common solvents, it can be obtained in pure form and then functionalized via Hagihara−Sonogashira coupling to give a series of highly ordered columnar liquid crystalline molecules **14a**−**c**. The total synthesis involves five 6-fold transformations, all in excellent to near quantitative isolated yields. Their thermotropic liquid crystalline behavior was studied by differential scanning calorimetry (DSC), polarized optical microscopy (POM) and wide-angle X-ray diffraction (WAXD). Compared to the normal alkyl-subsituted hexabenzocoronenes (HBCs), **14a**−**c** exhibit more highly ordered columnar mesophases, including three-dimensionally ordered superstructures (helical columnar mesophase). These could arise from additional intracolumnar $\pi-\pi$ interactions between, and space-filling requirements introduced by, the rigid-rod side groups. Atomic force microscopy (AFM) revealed self-assembled bundles of columnar aggregates in spin-coated films and isolated several-micron-long nanoribbons composed of a defined number of columns in drop cast films.

Introduction

Discotic columnar liquid crystalline materials with high one-dimensional charge carrier mobility along the columns show great promise as active components in organic electronics.[1] The realization of long range order through molecular design is surely one of the prime concerns.[2] This can be achieved via two general design principles: (1) alter the size, shape, or chemical makeup of the rigid molecular core, and, (2) introduce functionalities around the periphery which bring additional intracolumnar interaction, e.g., dipolar-coupling or hydrogen bonding.[2f,3] Examples of the former approach are alkyl- or alkylphenyl-substituted hexa-*peri*-hexabenzocoronenes (HBCs)[4] which possess a larger polycyclic aromatic hydrocarbon (PAH) core compared with other mesogens based on triphenylene,[2b,2d,5] porphyrin,[6] phthalocyanine,[7] etc. As a result, HBCs exhibit columnar mesophases with unusually high thermal stability, high order parameter,[4b] and high charge carrier mobility.[4d] Such properties make them likely candidates for organic semiconducting materials in field-effect transistors (FETs),[8] hole-conducting layers in photovoltaic devices[9] or light-emitting

† New address: University of Kentucky, Department of Chemistry, Lexington, Kentucky 40506-0055.

(1) Bushby, R. J.; Lozman, O. R. *Curr. Opi. Solid. State Mater. Sci.* **2002**, *6*, 569−578.
(2) (a) Adam, D.; Schuhmacher, P.; Simmerer, J.; Häussling, L.; Siemensmeyer, K.; Etzbach, K. H.; Ringsdorf, H.; Haarer, D. *Nature* **1994**, *371*, 141−143. (b) Fontes, E.; Heiney, P. A.; de Jeu, W. H.; *Phys. Rew. Lett.* **1988**, *61*, 1202−1205. (c) Idziak, S. H. J.; Heiney, P. A.; Mccauley, J. P.; Carroll, P., Jr.; Smith, A. B., III *Mol. Cryst. Liq. Cryst.* **1993**, *237*, 271−275. (d) Gramsbergen, E. F.; Hoving, H. J.; de Jeu, W. H.; Praefcke, K.; Kohne, B. *Liq. Cryst.* **1986**, *1*, 397−400. (e) Bock, H.; Babeau, A.; Seguy, I.; Jolinat, P.; Destruel, P. *ChemPhysChem* **2002**, *6*, 532−535. (f) Tang, B. Y.; Ge, J. J.; Zhang A.; Calhoun, B.; Chu, P.; Wang, H.; Shen, Z.; Harris, F. W.; Cheng, S. Z. D. *Chem. Mater.* **2001**, *13*, 78−86. (g) Glüsen, B.; Heitz, W.; Kettner, A.; Wendorff, J. H. *Liq. Cryst.* **1996**, *20*, 627−633. (h) Bayer, A.; Hübner, J.; Kopitzke, J.; Oestreich, M.; Rühle, W.; Wendorff, J. H. *J. Phys. Chem. B* **2001**, *105*, 4596−4602.
(3) (a) Sage, I. C. in *Handbook of Liquid Crystals*; Demus, D., Goodby, J., Gray, G. W., Spiess, H. W., Vill, V., Eds.; Wiley-VCH: Weinheim, 1998; Vol. 1, pp 731−762. (b) Levitsky, I. A.; Kishikawa, K.; Eichhorn, S. H.; Swager, T. M. *J. Am. Chem. Soc.* **2000**, *122*, 2474−2479. (c) Zheng, H.; Lai, C. K..; Swager, T. M. *Chem. Mater.* **1995**, *7*, 2067−2077. (d) Serrette, A. G.; Swager, T. M. *J. Am. Chem. Soc.* **1993**, *115*, 8879−8880. (e) Bushey, M. L.; Hwang, A.; Stephens, P. W.; Nuckolls, C. *Angew. Chem., Int. Ed.* **2002**, *41*, 2828−2831. (f) Paleos, C. M.; Tsiourvas, D. *Angew. Chem., Int. Ed.* **1995**, *34*, 1696−1711; Tsiourvas, D. *Angew. Chem., Int. Ed.* **1995**, *107*, 1839−1855. (g) Brunsveld, L.; Zhang, H.; Glasbeok, M.; Vekemans, J. A. J. M.; Meijer, E. W. *J. Am. Chem. Soc.* **2000**, *122*, 6175−6182.
(4) (a) Watson, M.; Fechtenkötter, A.; Müllen, K. *Chem. Rev.* **2001**, *101*, 1267−1300. (b) Herwig, P.; Kayser, C.; Müllen, K.; Spiess, H. W. *Adv. Mater.* **1996**, *8*, 510−513. (c) Stabel, A.; Herwig, P.; Mullen, K. *Angew. Chem., Int. Ed.* **1995**, *34*, 1609−1611; Stabel, A.; Herwig, P.; Mullen, K. *Angew. Chem., Int. Ed.* **1995**, *107*, 335−339. (d) van de Craats, A. M.; Warman, J. M.; Fechenkötter, A.; Brand, J. D.; Harbison, M. A.; Müllen, K. *Adv. Mater.* **1999**, *11*, 1469−1472. (e) Fechtenkötter, A.; Saalwächter, K.; Harbison, M. A.; Müllen, K.; Spiess, H. W. *Angew. Chem., Int. Ed.* **1999**, *38*, 3039−3042; Fechtenkötter, A.; Saalwächter, K.; Harbison, M. A.; Müllen, K.; Spiess, H. W. *Angew. Chem.* **1999**, *111*, 3224−3228. (f) Fechtenkötter, A.; Tchebotareva, N.; Watson, M.; Müllen, K. *Tetrahedron Symp.* **2001**, *57*, 3769−3783. (g) Samori, P.; Fechtenkötter, A.; Jäckel, F.; Böhme, T.; Müllen, K.; Rabe, J. P. *J. Am. Chem. Soc.* **2001**, *123*, 11 462−11 467. (h) Lee, M.; Kim, J.-W.; Peleshanko, S.; larson, K.; Yoo, Y.-S.; Vaknin, D.; Markutsya, S.; Tsukruk, V. V. *J. Am. Chem. Soc.* **2002**, *124*, 9121−9128. (i) Sadhukhan, S. K.; Viala, C.; Gourdon, A. *Synthesis* **2003**, *10*, 1521−1525. (j) Rathore, R.; Burns, C. L. *J. Org. Chem.* **2003**, *68*, 4071.
(5) Rego, J. A.; Kumar, S.; Ringsdorf, H. *Chem. Mater.* **1996**, *8*, 1402−1409.
(6) (a) Gregg, B. A.; Fox, M. A.; Bard, A. J. *J. Am. Chem. Soc.* **1989**, *111*, 1, 3024−3029. (b) Kimura, M.; Saito, Y.; Ohta, K.; Hanabusa, K.; Shirai, H.; Kobayashi, N. *J. Am. Chem. Soc.* **2002**, *124*, 5274−5275.
(7) (a) Piechoki, C.; Simon, J.; Skoulios, A.; Guillon, D.; Weber, P. *J. Am. Chem. Soc.* **1982**, *104*, 5245. (b) Chandrasekhar, S. *Mol. Cryst. Liq. Cryst.* **1981**, *63*, 171−180.
(8) (a) Kraft, A. *ChemPhysChem* **2001**, *2*, 163. (b) Katz, H. E.; Lovinger, A. J.; Johnson, J.; Kloc, C.; Siegrist, T.; Li, W.; Lin, Y.-Y.; Dodabalapur, A. *Nature* **2000**, *404*, 478.

Scheme 1. General Synthetic Route to the R-substituted HBCs

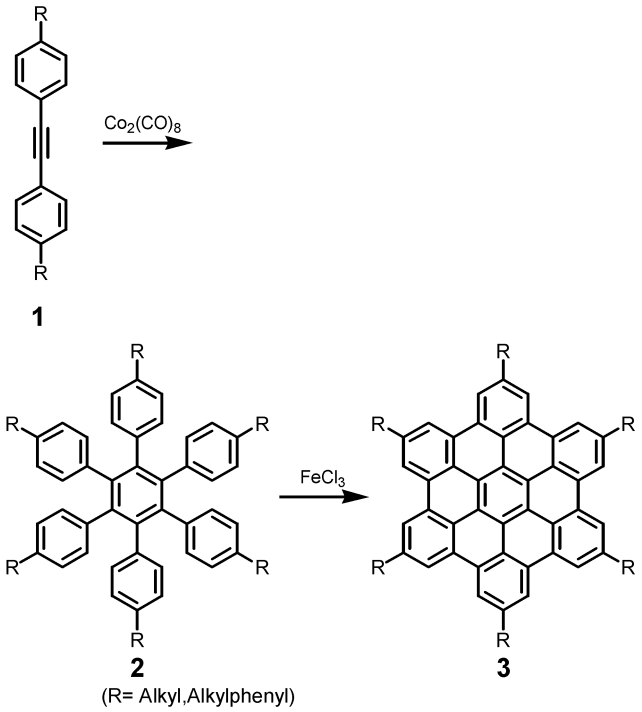

diodes (LEDs)[10] and molecular wires in nanoscale molecular electronics.[11] Two-dimensional crystals, self-assembled at surfaces by solution processing, have been visualized and electrically characterized by scanning tunneling microscopy (STM) or scanning tunneling spectroscopy (STS), respectively,[4c,4g] laying the groundwork for using them as molecular interfaces at electrode surfaces. Higher ordered structures both at interfaces and in the bulk have been realized by changing the nature of the pendant side chains.[4d,4g,12,13]

The synthesis of these molecules has been well established in our group and more recently pursued in others.[4c,4g,4h−j] As shown in Scheme 1, two key steps are involved in the synthesis of symmetrically substituted HBCs: (1) cobalt-catalyzed cyclotrimerization[14] of 4, 4′-substituted diphenylacetylenes **1** to substituted hexaphenylbenzenes **2**; and (2) oxidative cyclodehydrogenation of derivatives **2** with $FeCl_3$ to afford fused HBC derivatives **3**. Although this approach is simple, flexible, and provides the desired compounds in high yields in multigram scale, some drawbacks and limitations in its scope have been encountered. First, it requires the multistep synthesis of the substituted diphenylacetylenes **1** with the desired functionality "R". Carrying these substituents through subsequent steps can sometimes lead to lower atom economy. Second, the identity of "R" is limited by the tolerance of the cyclotrimerization catalyst as well as compatibility with the final oxidation step.[15,16]

Chart 1. Functionalizable HBC Building Blocks **4** and **5**.

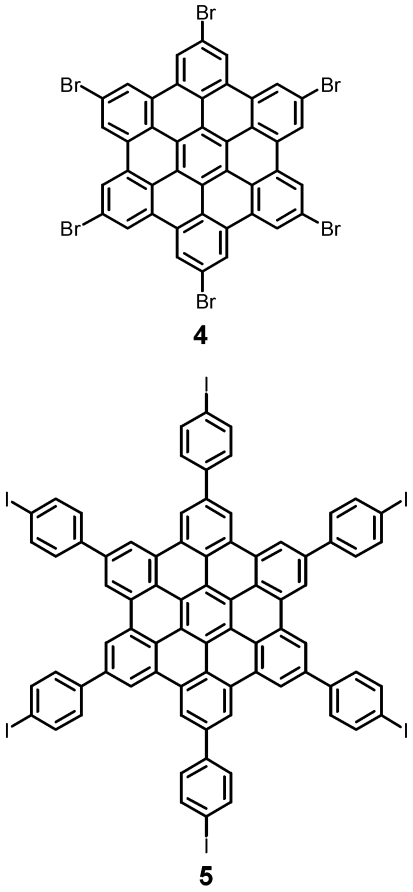

Direct attachment of heteroatoms such as oxygen, nitrogen, and sulfur to the HBC core is expected to modify self-assembly and electronic properties,[2a] however, attempted cyclodehydrogenation of alkoxy and alkylthio-substituted hexaphenylbenzenes resulted in ether cleavage.[17] In addition, electro-active moieties such as triarylamine are excluded presumably due to preferential formation of localized radical cations.[18]

For reasons of atom economy and to broaden the scope of our synthesis, we set out to prepare an HBC with versatile reactive sites, which can be converted by standard transition-metal catalyzed coupling reactions to a range of useful functionalities as a final synthetic step. The simplest target, compound **4** carrying six reactive bromine atoms, is being pursued with some success.[19] However, the nonfused peripheral rings of hexakis(4-iodophenyl)-*peri*-hexabenzocoronene **5** (Chart 1) were predicted to provide added value. Compared to *n*-alkyl substituents, 4-alkylphenyl groups impart the following characteristics: good solubility, longer-range order in the Col_h

(9) (a) Schmidt-Mende, L.; Fechtenkötter, A.; Müllen, K.; Moons, E.; Friend, R. H.; MacKenzie, J. *Science* **2001**, *293*, 1119−1122. (b) Tang, C. W. *Appl. Phys. Lett.* **1986**, *48*, 183.
(10) (a) Christ, T.; Glüsen, B.; Greiner, A. J.; Kettner, A.; Sander, R.; Stümpflen, V.; Tsukruk, V.; Wendorff, J. H. *Adv. Mater.* **1997**, *9*, 48−52. (b) Tang, C. W.; VanSlyke, S. A. *Appl. Phys. Lett.* **1987**, *51*, 913.
(11) Martin, R. E.; Diederich, F. *Angew. Chem, Int. Ed.* **1999**, *38*, 1350−1377; Martin, R. E.; Diederich, F. *Angew. Chem., Int. Ed.* **1999**, *111*, 1440−1469.
(12) Fischbach, I.; Pakula, T.; Minkin, P.; Fechtenkötter, A.; Müllen, K.; Spiess, H. W. *J. Phys. Chem. B* **2002**, *106*, 6408−6418.
(13) Brand, J. D.; Kübel, C.; Ito, S.; Müllen, K. *Chem. Mater.* **2000**, *12*, 1638−1647.
(14) Strukelj, M.; Papadimitrakopoulos, F.; Miller, T. M.; Rothberg, L. J. *Science*, **1995**, *267*, 1969.
(15) For example, attempted cyclotrimerization of bis(4-pyrimidyl)acetylenes catalyzed by $Co_2(CO)_8$ did not give any desired product.
(16) For example, standard cyclodehydrogenation of hexa (4-R-phenyl)benzenes with iron (III) chloride is so far unsuccessful with R = alkan-1-ones, alkoxycarbonyl, and methylene carboxy alkanoate.
(17) (a) Weiss, K.; Beernink, G.; Dötz, F.; Alexander, B.; Müllen, K.; Wöll, C. H. *Angew. Chem., Int. Ed.* **1999**, *38*, 3748−3742. *Angew. Chem.* **1999**, *111*, 3974−3978. (b) Fechtenkötter, A., Ph.D. Thesis, Johannes Gutenberg Universität, 2001.
(18) (a) Lambert, C.; Nöll, G. *Angew. Chem., Int. Ed. Engl.* **1998**, *37*, 2107−2110. *Angew. Chem., Int. Ed.* **1998**, *110*, 2239−2242. (b) Lambert, C.; Nöll, G. *Chem. Eur. J.* **2002**, *8*, 3467−3477.
(19) Attempted cyclodehydrogenation of hexa(4-bromophenyl)benzene with 36 eq. $FeCl_3$ gave, after 64h, a mixture of hexa(4-bromo)-*peri*-hexabenzocoronene, starting material, monochlorinated and dichlorinated hexa (4-bromo)-*peri*-hexabenzocoronene (MALDI-TOF).

mesophase, suppressing crystallization which can be undesirable for self-healing materials, and the highest reported charge-carrier mobility for a discotic liquid crystalline material.[4d,4e] Such a functionalizable core molecule is expected to provide the way to a new series of highly ordered liquid crystals and other electronic, optical, and magnetic active materials. Here, we present the remarkably simple and efficient synthesis of this key building block, and its subsequent functionalization by Hagihara-Sonogashira coupling[20] to give a series of highly ordered discotic liquid crystalline materials. *The total synthesis involves five 6-fold transformations, all in excellent to near quantitative yields*. Structural purity is established by mass spectrometry, NMR, UV−vis, and fluorescence spectroscopy, whereas self-assembly is characterized by differential scanning calometry (DSC), X-ray diffraction, polarized optical microscopy (POM) and atomic force microscopy (AFM). The materials self-assemble in the bulk to highly ordered columnar mesophases including a rare helical phase and from dilute solution to well-defined nanostructures such as nanowires and nanoribbons.

Results and Discussion

Synthesis of Hexa(4-iodophenyl)-*peri*-hexabenzocoronene (5). The synthesis of hexakis(4-iodophenyl)-*peri*-hexabenzocoronene (**5**) is outlined in Scheme 2. The precursor hexakis-(4-iodophenyl)-hexaphenylbenzene (**12**) was prepared in 92% isolated yield by reaction of excess iodine monochloride with hexakis(4-trimethylsilylphenyl)hexaphenylbenzene (**9**), which was synthesized via two different routes. The first (convergent) route begins with the Stille coupling[21] between **4**, bis-(4-bromophenyl)acetylene (**6**)[4e] and 4-(trimethylsilyl)-1-(trimethylstannyl)benzene (**7**),[22] to give bis{4[4-(trimethylsilyl)-phenyl]phenyl}acetylene (**8**) in 75% yield. The product precipitates during the reaction, rendering the good yield as well as simple purification. Hexakis{4[4-(trimethylsilyl)phenyl]-phenyl}benzene (**9**) was then prepared by $Co_2(CO)_8$-catalyzed cyclotrimerization of compound **8** in 92% isolated yield. To avoid organotin chemistry as well as to simplify the synthetic route, an alternate (divergent) route was developed. By slight modification of a reported procedure,[23] commercially available hexaphenylbenzene (**10**) was selectively brominated in neat bromine to afford hexakis(4-bromophenyl)benzene (**11**) in quantitative yield. Compound **9** was then prepared by 6-fold Suzuki coupling[24] between **11** and excess commercially available 4-trimethylsilylbenzeneboronic acid in 92% yield. All of these soluble compounds were fully characterized by NMR and mass spectrometry techniques. The crucial final cyclodehydrogenation step was completed by treating **12** with iron (III) chloride, dissolved in nitromethane, in a 2:1 dichloromethane (DCM)/CS_2 solvent mixture instead of pure DCM (standard for this reaction) to facilitate reaction of the poorly soluble starting material. The final product **5** was obtained in quantitative yield as a yellow powder, after quenching/precipitation and repeated washing with methanol. The vanishing solubility of **5** precludes ^{1}H NMR and ^{13}C NMR characterization. High-resolution MALDI MS, following solid-state analyte-in-matrix preparations,[25] reveals a single species with isotopic distribution in accord with that calculated for compound **5** (see the Supporting Information). Further structural proof is not necessary as subsequent functionalization imparts solubility facilitating full spectral characterization.

Synthesis and Characterization of a Series of Discotic Liquid Crystalline Materials from Building Block 5. Naturally, the next step is to probe the potential of **5** as a chemical as well as physical building block for novel molecular materials, specifically discotic columnar liquid crystalline materials. Despite the virtual insolubility of compound **5**, Hagihara−Sonogashira coupling reactions with solubilizing acetylenes **13a**−**c** is possible, thus paving the way to versatile functionalization. As outlined in Scheme 2, cross-coupling between **5** and **13a**−**c** in piperidine, followed by standard column chromatography, gives a series of soluble extended HBC derivatives **14a**−**c** in good yield. MALDI-TOF analyses of the crude reaction mixtures indicate only one HBC product in each case, and therefore the lower isolated yields may reflect losses during purification. HBC **14a** has a structure similar to the recently reported hexakis(4-dodecylphenyl)-*peri*-hexabenzocoronene[4e] but with additional acetylenic linkages, which can modify self-assembly, as well as serving as reactive sites for further functionalization.[26] Compounds **13b,c** were chosen to extend the rigidity of the mesogenic core, in hopes of inducing more ordered superstructures due to interlocking of the rigid-rod like arms. **13b** was prepared according to the literature.[17a] Compound **13c**, with its three long alkoxy chains, was prepared as shown in Scheme 3. Commercially available 3, 4, 5-trimethoxybromobenzene was demethylated with BBr_3 to give 1-bromo-3,4,5-trihyroxybenzene, which was immediately alkylated with *n*-dodecylbromide to give 1-bromo-(3,4,5-tridodecoxy)benzene (**15**) in 85% isolated overall yield. Standard Hagihara-Sonogashira coupling between compound **15** and trimethylsilylacetylene followed by desilylation gave **13c** in near quantitative overall yield. The disklike molecules **14a**−**c** exhibit good solubility in common solvents, facilitating their full structural characterization. High resolution MALDI MS proved that 6-fold Hagihara-Sonogashira coupling could be easily fulfilled without competing reduction of the aryl iodide moieties (see the Supporting Information). Isotopic distributions are also in agreement with the simulation results, further proving the fully fused structure of compound **5**.

The relative tendencies of compounds **14a**−**c** to aggregate in solution were assessed qualitatively by solution NMR and optical spectroscopy. Variable-temperature ^{1}H NMR spectra for compounds **14a**−**c** were collected in deuterated 1,1,2,2-tetrachloroethane with the same concentration (see the Supporting Information). In all cases, the singlet resonances arising from the protons attached to the HBC cores progressively shift to lower fields with increasing temperature, indicating aggregation equilibria.[27] At 413 K, the chemical shifts for these protons are 8.1, 7.4, and 9.26 ppm for **14a**, **14b**, **14c** respectively, indicating that **14b** has the strongest while **14c** has the weakest aggregation. Solution UV−vis absorption and photoluminescence spectra

(20) (a) Taskahashi, S.; Kuroyama, Y.; Sonogashira, K.; Hagihara, N. *Synthesis* **1980**, 627. (b) Bunz, U. H. F. *Chem. Rev.*, **2000**, *100*, 1605−1644.
(21) (a) Mitchell, T. N. *Synthesis* **1992**, 803. (b) Ritter, K. *Synthesis* **1993**, 735.
(22) Nitschke, J. R.; Zürcher, S.; Tilley, T. D. *J. Am. Chem. Soc.* **2000**, *122*, 10 345−10 352.
(23) Rathore, R.; Burns, C. L.; Deselnicu, M. I. *Org. Lett.* **2001**, *3*, 2887−2890.
(24) (a) Miyaura, N.; Yanagi, T.; Suzuki, A. *Synth. Commun.* **1981**, *11*, 513; b) Miyaura, N.; Suzuki, A. *Chem. Rev.* **1995**, *95*, 2457.
(25) Przybilla, L.; Brand, J. D.; Yoshimura, K.; Räder, J.; Müllen, K. *Anal. Chem.* **2000**, *72*, 4591.
(26) Diels−Alder cylcloaddition of functionalized tetraphenylcyclopentadienones to the acetylenic linkages of **14a** occurs readily.

Scheme 2. Synthesis of Compound **5**

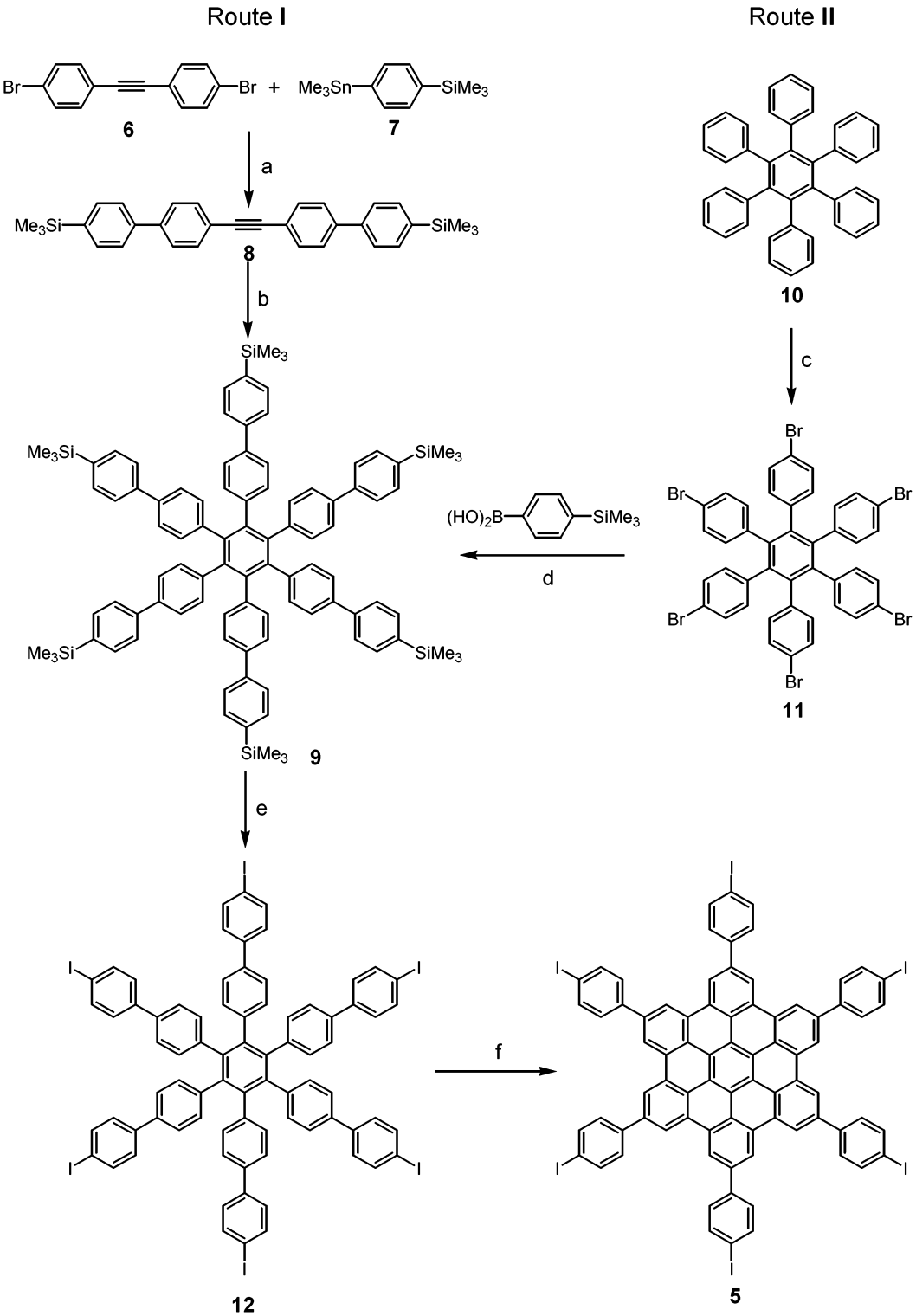

(a) $Pd(PPh_3)_4$, toluene, 125 °C,75%; (b) $Co_2(CO)_8$, dioxane, 125 °C, 92%; (c) neat bromine, −20 °C to room temperature, 96%; (d) $Pd(PPh_3)_4$, K_2CO_3(aq.), 95 °C, 92%; (e) ICl, chloroform, 92%; (f) $FeCl_3$/nitromethane, DCM/CS_2 = 2:1.

(THF, 1.0×10^{-6} M and 5×10^{-7} M, respectively) of compounds **14a**−**c** are shown in Figure 1. The absorption maxima (λ_{max}) were 380, 386, and 387 nm respectively, each red-shifted over 15 nm compared to *n*-alkyl-substituted HBCs (λ_{max} = 365 nm). This can be explained by some electronic communication between the HBC core and the phenylacetylene or diphenylacetylene substituents. Alternately, the bulky side groups may bias the time-averaged orientation of the disks relative to each other within aggregates, modifying intermolecular orbital interaction.[28] Absorption bands centered at 268 nm (**14a**), 295 nm (**14b**) and 293 nm (**14c**) could be assigned to the phenylacetylene and tolane moieties, respectively. Differences in the fluorescence spectra for **14a**−**c** support the above conclusions regarding aggregation based on NMR studies.

Scheme 3. Synthesis of Extended HBC Derivatives **14a−c**

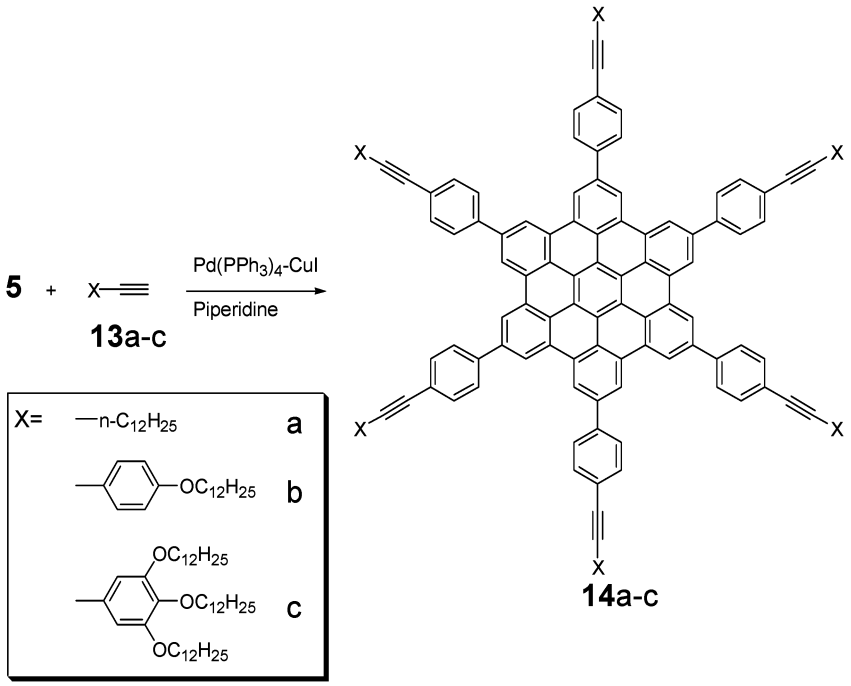

Scheme 4. Synthesis of Monoethynylenes **13c**

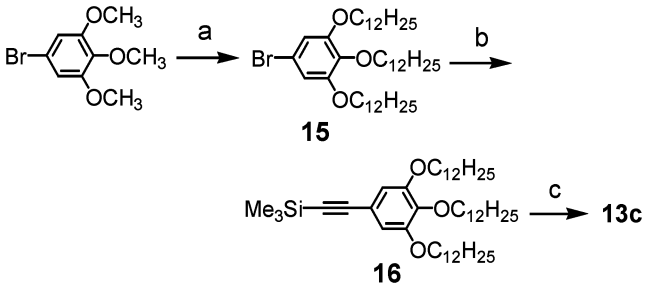

(a) BBr_3; $H_{25}C_{12}Br$, K_2CO_3, 85%; (b) trimethylsilylacetylenes, Pd-$(PPh_3)_4$−CuI, piperidine, 80 °C, 92%; (c) K_2CO_3, DCM/Methanol, 96%.

Compound **14b** gives a broad unstructured emission centered at 533 nm, significantly red-shifted compared to compounds **14a** and **14**c, as well as *n*-alkyl substituted HBCs. The emission spectrum of **14c** is virtually identical to *n*-alkyl substituted HBCs and with greater intensities than compounds **14a** and **14b**, indicating lower degree of aggregation. Although additional $\pi-\pi$ interactions of the diphenylacetylene arms may impart a greater tendency of **14b** to aggregate, the additional 12 dodecyloxy chains of **14c** may negate this effect sterically or entropically.

Thermotropic Liquid Crystalline Behavior of 14a−c. The bulk thermotropic liquid crystallineproperties of **14a−c** were investigated by differential scanning calorimetry (DSC), polarized optical microscopy (POM), and wide-angle X-ray diffraction (WAXD, extending down to intermediate angles). A summary of the phase transition temperatures and X-ray mesophase analysis is outlined in Table 1 and Table 2,

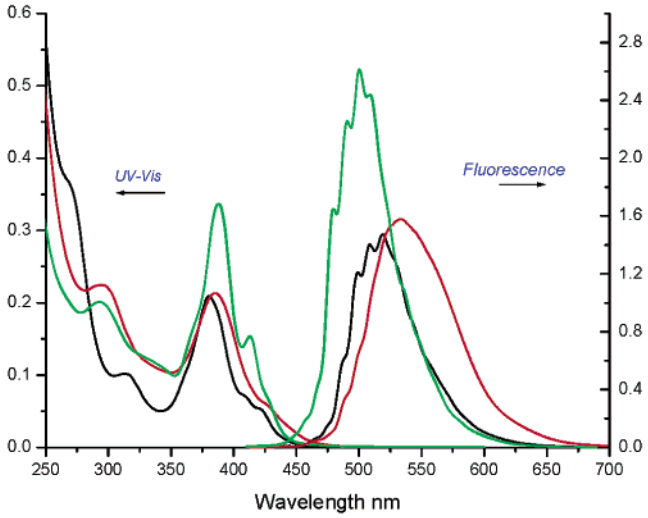

Figure 1. Combined UV−vis and fluorescence spectra of compounds **14a−c** recorded at room temperature in 1.0×10^{-6} M and 5×10^{-7} M THF solution, respectively. Black line: **14a**; red line: **14b** and green line: **14c**.

respectively. Compounds **14a−c** were extruded[12] to oriented filaments (coincident fiber/columnar axes), and WAXD patterns in transmission were recorded with vertical orientation of the filament axis and with the beam perpendicular to the filaments.

As is the case for most HBCs, no clearing point was observed by POM below 400 °C for compounds **14a−c**, indicating highly thermally stable mesophases, and no true crystalline phases. Thin films were prepared by drop casting (1% toluene) and observed between crossed polarizers (Figure 2). The characteristic fanlike texture typically observed for hexagonal columnar mesophases,[29] could not be developed because the samples could not be first melted. The mosaic-like texture observed for **14c** is typical of highly ordered Smectic liquid crystals or plastic crystals.[30] In

(27) (a) Zhang, J.-S.; Moore, J. S. *J. Am. Chem. Soc.* **1992**, *114*, 9701−9702. (b) Abraham, R. J.; Eivazi, F.; Pearson, H.; Smith, K. M. *J. Chem. Soc., Chem. Commun.* **1976**, 698−699. (c) Shetty, A. S.; Zhang, J.-S.; Moore, J. S. *J. Am. Chem. Soc.* **1996**, *118*, 1019−1027. (d) Tobe, Y.; Utsumi, N.; Kawabata, K.; Nagano, A.; Adachi, K.; Araki, S.; Sonoda, M.; Hirose, K.; Naemura, K. *J. Am. Chem. Soc.* **2002**, *124*, 5350−5364.

(28) Cornil, J.; Lemaur, V.; Calbert, J.-P.; Brédas, J.-L. *Adv. Mater.* **2002**, *14*, 726−729.

(29) Demus, D.; Richter, L. *Texture of Liquid Crystals*, 1st ed.; Weiheim: New York, 1978.

Table 1. Phase Transition Data of **14a**−**c** from DSC[a]

	T(°C) and [Δ*H*(kJ/mol)]		
	first heating	first cooling	second heating
14a	Col_1 2.04 °C[−13.16] Col_2 19.8 °C[−6.8]D_h	D_h −4.8 °C]26.85]Col_1	Col_1 2.86[−10.37] Col_2 19.54 [−6.25] D_h
14b	D_{hh}85.8 °C [−12.19] D_h	D_h 44.4 °C [8.35] D_{hh}	D_{hh} 76.80 [−11.95] D_h
14c	Col_3 17.7 °C [−27.92] Col_4 48.2 °C[−42.28] D_{hh} 74.40 [−22.43] *D*	D_h 69.3 °C [13.62] D_{hh} 11.5 °C[110.3] Col_3	Col_3 19.0 °C [−98.71] D_{hh} 74.4 °C [−13.6] D

[a]Abbreviations: Col_n for unassigned columnar phase, D_{hh} for discotic columnar hexagonal helical, D_h for discotic columnar hexagonal columnar liquid crystalline phase, and D for unclear disordered columnar phase.

Table 2. Data Collected from 2D X-ray Diffraction Patterns of **14a**−**c**

	2D WAXD from extruded fibers	
	Miller index	*d* spacing (□)
14a	100	29.40
	110	17.18
	200	14.42
	210	10.88
	001	3.47
14b	100	31.72
	110	18.21
	200	15.92
	004	3.45
14c	100	45.42
	110	30.36
	200	22.71
	210	17.2
	300	15.2
	004	3.47
	001	14.9

the case of **14b**, only weak birefringence is observed at room temperature or elevated temperature up to 450 °C. However, after simple shearing the as-prepared film in one direction, a clear stripe-like birefringence is observed as shown in Figure 2b.

To further investigate the thermotropic mesophase behavior of **14a**−**c**, temperature-dependent 2D WAXD data was collected from oriented samples within the different thermal phases defined by transitions observed by DSC (DSC data, see Supporting Information). The selected 2D X-ray diffraction patterns for **14a,b** at varying temperatures are shown in Figure 3. From DSC measurements, HBC **14a** undergoes two 1st order endothermic transitions with peak values of 3 °C and 20 °C. Comparison with the analogous HBC **3a** (R = 4-Ph$C_{12}H_{25}$; endothermic transitions at 15 °C and 80 °C) reveals distinct differences introduced by the small structural change of inserting acetylenic linkages into the side chains. HBC **3a** forms columnar mesophases from below room temperature, which persist to well above 300 °C where decomposition begins. The columns are arranged in a square 2D lattice within the thermal window defined by the two endothermic transitions, and in a hexagonal columnar liquid crystalline (**D_h**) above.[12] The 2D WAXD pattern for **14a** at room temperature, Figure 3a, reveals also a **D_h** mesophase. The two intense, symmetric meridianal arcs indicate face-to-face stacking (d = 0.347 nm) of disks with their molecular planes perpendicular to the orientation/columnar axes. A set of well-resolved equatorial arcs with relative reciprocal spacing of $1:\sqrt{3}:\sqrt{4}$ define the lateral hexagonal packing of the columns. The thermal transition to the hexagonal packing arrangement is substantially reduced in the case of **14a** compared to **3a**, and the width of the phase window between the two endothermic peaks is so narrow that it is not practically accessible.

Above its single detectable endothermic transition at ∼86°, **14b** is arranged in a similar **D_h** mesophase (2D WAXD, see the Supporting Information). Upon cooling to room-temperature many additional reflexes forming parabolic layer lines appear (Figure 3b), the number and intensity of which increase with slower cooling indicating greater structural perfection. Multiple representations with varying contrasts are necessary to visualize the maximum number of reflections (see the Supporting Information). The first layer above/below the equator (l = 1) corresponds to a repeating distance along the columns which is exactly four times the $\pi-\pi$ stacking distance separating disks, indicating that every 5th disk within a column is positionally/rotationally correlated. Given the hexagonal symmetry of the molecule, such a correlation can be realized by rotating each successive centrosymmetrically stacked disk by 15° (azimuthal) about the columnar axis leading to a helical stacking in which pairs of disks separated by three intervening disks are rotationally eclipsed. Simulation[31] of the 2D WAXD pattern expected from a hexagonal packing of such helical columns (with lattice constant defined by the experimental equatorial reflections) and the corresponding model of a short helical columnar segment are shown in Figure 3c,d. Overall, there is good agreement between the experimental and simulated diffractograms but with some deviation in positions and relative intensities of cross-peaks due to uncertainty in the lateral and oblique correlations between disks in neighboring columns. SAXD measurements reveal reflexes at intermediate angles (approaching 10 nm distances, not shown) suggesting a long-range columnar superstructure superimposed on the local hexagonal packing, however, more detailed analysis will be the subject of future investigations.

An oriented sample of **14c**, annealed at 120 °C for 2 h and slowly cooled to room temperature also exhibits a 3D superstructure (see the Supporting Information) of helical columns such as that of **14b**. In contrast to **14a,b**, the relative intensities of the (110) and (200) reflections are much weaker in **14c** which could be related to different oblique 3D intercolumnar correla-

(30) (a) Sackmann, H.; Demus, D. *Mol. Cryst. Liq. Cryst.* **1973**, *21*, 239. (b) Demus, D.; Diele, S.; Klapperstück, M.; Link, V.; Zaschke, H. *Mol. Cryst. Liq. Cryst.* **1971**, *15*, 161.

(31) Calculations made with *Cerius 2* software based on the helical columns as in Figure 3d, packed in a hexagonal lattice with a = 3.78 nm (determined from 2D X-ray experimental data) with alkyl chains all-trans (misorientation of alignment 5∼7%).

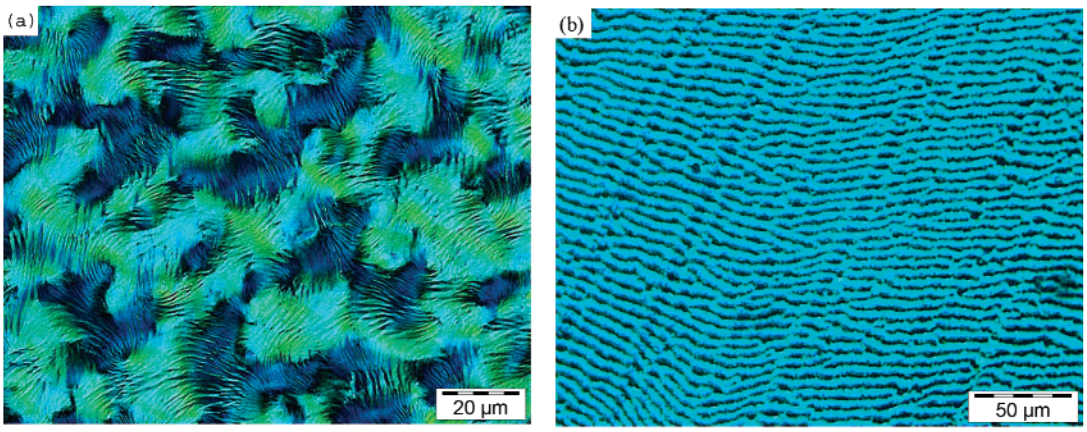

Figure 2. Typical optical textures of (a) **14c** at 25 °C. b) **14b** at 290 °C, from the sheared film. The shearing direction is perpendicular to the stripes in the texture.

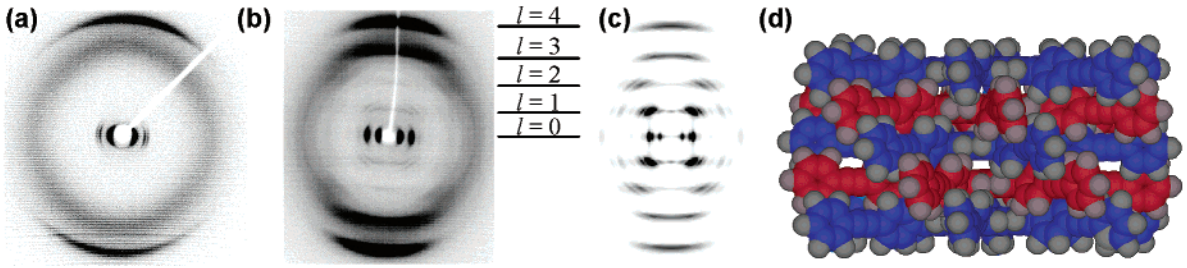

Figure 3. 2D X-ray diffraction patterns for extruded fibers of (a) **14a** and (b) **14b** at room temperature. (c) 2D WAXD calculated[31] based on hexagonal packing of the proposed helical column shown at left. (d) Proposed helical stacking for compounds **14a,b** with each successive disk rotated by 15° about the columnar axis. Every 5th disk is rotationally eclipsed. Alkoxy chains omitted for clarity. In all cases, column and/or fiber axes vertical.

tions. When recorded at 130 °C, all meridianal reflections are replaced by diffuse and split reflections flanking the meridian (see the Supporting Information). At the same time, we see only two equatorial reflections with an approximate reciprocal spacing ratio of $1:\sqrt{7}$. Exact assignment of columnar liquid crystalline phase is not possible due to lack of more reflection peaks. It can be assumed that the very bulky trialkoxy phenyl substituents (wedge-shape) disrupt the stacking upon rotation of the disk cores yielding the diffuse and split reflections seen flanking the meridian in the WAXD diffractogram. It should also be noted that the superstructures seen for **14b** and **14c** are not observed in the as-extruded fiber of the latter, i.e., without annealing and slow cooling from above 100 °C. Again, the more bulky wedge-shaped side groups of **14c** are responsible, requiring sufficient thermal energy and time to reorder into the superstructure.

It can generally be assumed that efficient columnar packing of "thin" (~0.35 nm) discotic mesogens requires successive disks to be rotated relative to each other to accommodate the "thicker" side chains. Although there are many reports in which circular dichroism indicates helical stacking, both in solution and bulk, induced by chiral centers in the side chains,[4f,32] it is otherwise relatively rare to experimentally observe a helical arrangement by diffraction.[2b,33,34] A helical 3D ***crystalline*** phase, observed from a hexa-thioalkyl triphenylene, brings with it exceptional one-dimensional charge-carrier mobilities along the columns.[2a] In a similar case, hexaester substituted triphenylenes also form a helical crystalline phase, i.e., every 5th disk in the column is correlated by rotating 30° between the neighboring disks.[34] Preliminary studies also indicate that such a phase is present in HBC **3a** at very low temperatures, where thermal energy in sufficiently reduced and disk rotation ceases. "Fast" rotation of the disks about their common columnar axes in the high-temperature phase is substantially slowed in the room-temperature phase as determined by solid-state NMR.[12]

The ***noncrystalline*** helical arrangement observed here at room temperature for **14b,c** is attributed to the rigid diphenylacetylene arms which leave a large empty wedge that can be filled efficiently when disks are rotated successively by 15°. Hypothetically, rotation of the inner and outer phenyl rings (+25° and −15°, respectively) out of the plane of the central core places these exo-phenyl rings from successive molecules face-to-face and separated by 0.34−0.38 nm, ideal for additional stabilizing $\pi-\pi$ interactions. The low intensity of the (off)meridianal reflections observed in the intermediate angle region, associated with the superstructure, together with the materials' susceptibility to plastic deformation (extrusion) clearly indicates noncrystalline phases. Preliminary solid-state NMR measurements (not shown) reveals various molecular mobilites. Because this phase is distinguished from the typical crystalline phase and disordered liquid crystalline phase, we would like to assign it as a 3D ordered plastic crystalline phase. It should be pointed out that a helical columnar liquid crystalline phase was recently claimed for a series of self-organized dendrimers reported by Percec et al.[35] The unique helical plastic crystalline phase disclosed here represents a new superstructure in the discotic materials. In anticipation of exploiting this arrangement

(32) (a) Goodby, J. W. *J. Mater. Chem.* **1991**, *1*, 307. (b) Praefcke, K.; Eckert, A.; Blunk, D. *Liq. Cryst.* **1997**, *22*, 113; van Nostrum, C. F., *Mol. Cryst. Liq. Cryst.* **1997**, *302*, 303.
(33) Charra, F.; Cousty, J. *Phys. Rev. Lett.* **1998**, *80*, 1682−1685.
(34) Voigt-Martin, I. G.; Garbella, R. W.; Schumacher, M. *Liq. Cryst.* **1994**, *17*, 775−801.

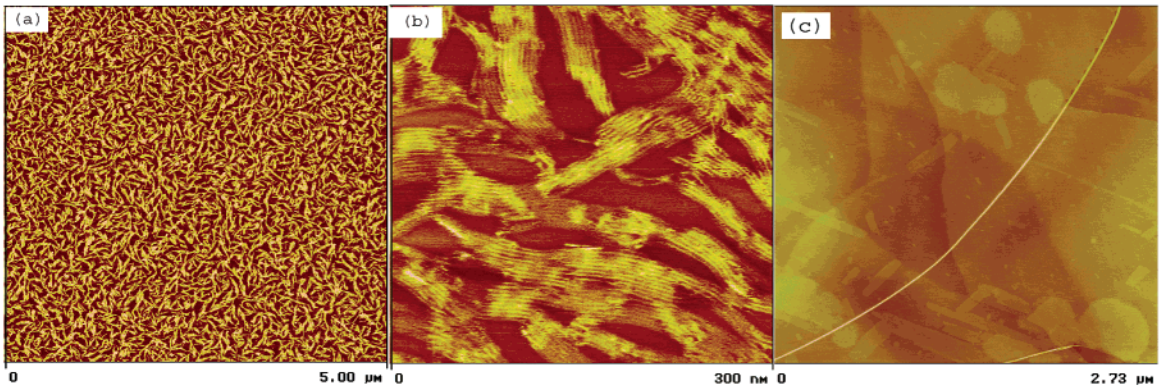

Figure 4. Typical tapping mode AFM images on HOPG surfaces: (a) **14a**, a spin-coated film from 1 mg/ml chloroform solution, phase mode in 5 μm scan size; (b)**14a**, phase mode in 300 nm scan size; (c) Nanoribbon from drop-cast solution of **14b** from 1% THF solution, (height mode in 2.73 μm scan size). Ribbon is ~21 nm wide and 3.8 nm high.

to get additional pathways for charge transport, the preparation of analogous HBC's in which the rigid-arms are replaced with ones having electronic function, e.g., traditional hole or electron conducting materials, is underway.

Self-Assembly from Solution: AFM Studies. The highly ordered structures of **14a**−**c** in the bulk state disclosed above prompted us to further study the self-assembly of **14a**−**c** at the nanoscale by atomic force microscopy (AFM). Here, we show the high tendency of **14a**−**c** to self-assemble to ordered nanoobjects such as nanorods and nanoribbons from solution. Typically, solutions in chloroform with varying concentrations were spin coated onto freshly cleaved HOPG substrates. In the case of **14c**, fairly uniform monolayer coverage was obtained and AFM scans (tapping mode) showed wormlike oriented domains (see the Supporting Information). Each domain is a composite of several parallel oriented nanorods, which typically extend over tens to hundreds of nanometers with average widths of 10~11 nm.

Selected AFM images for the solvent cast films of **14a** are shown in Figure 4a,b with scan sizes of 5 μm and 300 nm, respectively. Stripe-like domains extending over tens to hundreds of nanometers with different orientations were observed. Section analysis (Figure 4b) with higher magnification reveals that these domains are further composed of arrays of parallel stripes with widths of ~3.4 nm. This corresponds to the intercolumnar spacing in the bulk mesophase of **14a** determined by WAXD measurements. The height of the stripes also corresponds to the calculated molecular diameter in the discoid plane, so each stripe represents a single column of molecules, which are oriented with the columnar axis approximately parallel to the substrate.

The spin-coated film of **14b** also showed ordered superstructures composed of long rope-like domains (see the Supporting Information). Alternately, a solvent-cast film of **14b** on HOPG was prepared by drop-casting followed by slow evaporation of the solvent according to a literature method[36] in order to increase the time-scale for self-assembly. Nanoribbons extending over several micrometers in length with regular width and height were observed, as shown in Figure 4c. Section analysis of this ribbon showed that the width is ~21 nm and the height is ~3.8 nm, so we interpret the ribbon as an array of 5−6 parallel single columns with edge-on orientation. The mechanism of the nanofiber formation could be related to the strong intracolumnar $\pi-\pi$ interaction as well as intercolumnar packing noted by WAXD measurements of the bulk material as described above. Similar fiber formation has been observed from drop-cast films of polyphenylene dendrimers and in other conjugated systems.[36,37]

This strong tendency toward self-assembled well-defined nanowires in ultrathin films makes these materials highly promising candidates for nanoscale electrical and optical devices. Of course controlled orientation of these features is necessary for such considerations, and we are currently approaching this task by utilizing different substrates.

Conclusions

A hexa-*peri*-hexabenzocoronene core **5** carrying six reactive sites can be prepared by a rational approach and subsequently easily and quantitatively functionalized by standard transition metal-catalyzed coupling reactions. A remarkable feature of the synthesis presented here is that it involves several quantitative 6-fold chemical transformations, two of which occur despite either an insoluble product or insoluble starting material. It allows functionalization as a final step, which enhances atom economy and is predicted to greatly broaden the scope of functionalities which may be incorporated. The pendant aryl iodides of this new building block will allow capitalization of the rich chemistry associated with transition metal-catalyzed coupling reactions (Suzuki, Buchwald, Kumada, etc.) paving the way to a whole new series of HBC-based optical-, electronic- and magnetic- active liquid crystalline materials. The principle was demonstrated through the preparation of a series of HBCs with extended rigid cores resulting in self-assembly to more highly ordered columnar superstructures in the bulk state and to nanoscale structures from solution. In addition, the carbon−carbon triple bonds in **14a**−**c** provide active sites for further functionalization, e.g., by Diels−Alder cycloaddition or covalent fixation, subjects of current investigation. Current efforts also focus on attachment of functional π-systems (n- or p-type

(35) Percec, V.; Glodde, M.; Bera, T. K.; Miura, Y.; Shiyanovskaya, I.; Singer, K. D.; Balagurusamy, V. S. K.; Helney, P. A.; Schnell, I.; Rapp, A.; Spiess, H.-W.; Hudson, S. D.; Duan, H. *Nature* **2002**, *419*, 384−387.

(36) Liu, D.; Zhang, H.; Grim, P. C. M.; De Feyter, S.; Wiesler, U.-M.; Berresheim, A. J.; Müllen, K.; De Schryver, F. C. *Langmuir* **2002**, *18*, 2385−2391.

(37) Schenning, A. P. H. J.; Kilbinger, A. F. M.; Biscarini, F.; Cavallini, M.; Cooper, H. J.; Derrick, P. J.; Feast, W. J.; Lazzaroni, R.; Leclere, Ph.; McDonell, L. A.; Meijer, E. W.; Meskers, S. C. J. *J. Am. Chem. Soc.* **2002**, *124*, 1269−1275.

(photo)semiconductors) such that the whole can lead to nanoscale coaxial cables.

Experimental Section

General. ^{1}H NMR and ^{13}C NMR spectra were recorded in deuterated solvents such as CD_2Cl_2 and $C_2D_2Cl_4$ on a Bruker DPX 250 and Bruker DRX 500. UV−vis spectra were recorded on a Perkin-Elmer Lambda 9 spectrophotometer at room temperature. Fluorescence spectra were recorded on a Spex Fluorolog II (212). FD mass spectra were obtained on a VG Instruments ZAB 2-SE-FPD. High-resolution MALDI mass spectra were recorded on a Bruker Reflex II-TOF Spectrometer using a 337 nm nitrogen laser with TCNQ as matrix.[25] Elemental analysis was carried on a Foss Heraeus-Vario EL. Differential scanning calorimetry (DSC) was measured on a Mettler DSC 30 with heating and cooling rate of 10 K/min. A Zeiss Axiophot with a nitrogen flushed Linkam THM 600 hot stage was used to characterize optical textures. Powder wide-angle X-ray diffraction (WAXD) experiments were performed using a Siemens D 500 Kristalloflex with graphite-monochromatized CuKα X-ray beam, emitting from a Rigaku RV-300 rotating anode. 2-D X-ray diffraction of oriented fibers was conducted using a rotating anode (Rigaku, 18 kw) X-ray beam (CuKα, pinhole collimation, double graphite monochromator) with the beam perpendicular to the fiber axis and CCD or Kissig film camera. All of the AFM measurements were made using tapping mode operation on a Nanoscope IIIa Multimode scanning probe microscope from Digital Instruments (Santa Barbara, CA) using an "E" vertical engage scanner. Tapping mode etched silicon probes (manufacturer specifications: spring constant $k_0 = 39\sim69$ N/m, force constant $f_0 = 336\sim402$ kHz) with about 5∼10 nm radiuses were used for imaging. Melting points were measured on Büchi B-545 with a gradient rate of 2 °C/min (uncorrected).

Unless otherwise noted, all starting materials were purchased from Aldrich, Acros, ABCR, and used as received. THF and toluene for water-free reactions were refluxed over potassium under argon and freshly distilled before use.

Bis{4[4-(trimethylsilyl)phenyl]phenyl}benzene(8). In a 100-mL two-neck flask, 3.865 g bis(4-bromophenyl)acetylene (**6**) (11.5 mmol), 18 g **7** (57.5 mmol), 398 mg $Pd(PPh_3)_4$ (1.5 mol % per Br) and 30 mL dry toluene were combined. The mixture was degassed by two "freeze−pump−thaw" cycles and then heated to 125 °C for 48 h. Upon cooling to RT, white platelike crystals formed and were collected by suction filtration. The solid was washed with 10 mL dichloromethane, dried under reduced pressure to give 4.1 g (75.1%) analytically pure **8**. mp 275.3 °C. ^{1}H NMR (250 MHz, $C_2D_2Cl_4$): δ ppm 7.55 (m, 16H), 0.23 (s, 18H). ^{13}C NMR (125 MHz, $C_2D_2Cl_4$): δ ppm −0.71, 90.20, 122.38, 126.54, 127.27, 132.44, 134.31, 140.02, 140.31, 140.51. FD-MS (8 KV): *m*/*z* 474.6, calcd. 474.8. Elemental analysis: Calcd: C 80.95, H 7.22, Si 11.83; Found: C 80.96, H 7.24.

Hexakis{4[4-(trimethylsilyl)phenyl]phenyl}benzene (9) (Route I). 3.8 g compound **8** (8.0 mmol) was dispersed in 300 mL degassed dioxane, and 273.5 mg $Co_2(CO)_8$ (10 mol %) was added. The mixture was heated to 125 °C for 7 h under argon and concentrated under reduced pressure. Column chromatography (silca gel, PE/DCM = 7:3) gave 3.5 g (92%) white powder as pure product. mp 400.1 °C. ^{1}H NMR (250 MHz, $C_2D_2Cl_4$): δ ppm 0.22 (s, 54H), 6.87 (d, J = 8.2 Hz, 12H), 7.09 (d, J = 8.2 Hz, 12H), 7.31 (d, J = 8.2 Hz, 12H), 7.38 (d, J = 8.2 Hz, 12H). ^{13}C NMR (125 MHz, $C_2D_2Cl_4$): δ ppm −0.74, 125.53, 126.24, 132.26, 133.93, 137.12, 139.09, 140.23, 140.28, 140.98. FD-MS (8 KV): *m*/*z* 1424.60, calcd. 1424.40. Elemental analysis: Calcd. C 80.95, H7.22, Si 11.83; Found: C 80.94, H7.23.

Hexakis{4[4-(trimethylsilyl)phenyl]phenyl}benzene (9) (Route II). 3.27 g Hexakis(4-bromophenyl)benzene **11** (3.24 mmol), 5.67 g 4-trimethylsilylbenzeneboronic acid (29.2 mmol), 450 mg $Pd(PPh_3)_4$, 100 mL 1 M aqueous K_2CO_3 solution and 200 mL toluene was mixed and degassed by argon sparge. The mixture was heated to reflux overnight under argon and cooled. The organic layer was diluted with 100 mL toluene, washed with water (50 mL × 3), and dried over magnesium sulfate. Workup and purification then proceeded as above. 4.24 g (92%) pure compound was obtained.

Hexakis(4-bromophenyl)benzene (11). A 25-mL Schlenk tube filled with 2 g hexaphenylbenzene and a stirring bar was cooled to −20 °C, to which 3 mL of neat Br_2 was added dropwise. The mixture was slowly warmed to RT over 1 h, stirred for another 2 h, and then poured into 10% aqueous sodium disulfite. The white solid was collected and washed by water and acetone, dried under reduced pressure to give 3.6 g (96%) white powder **11**. mp 400.1 °C. ^{1}H NMR (500 MHz, $C_2D_2Cl_4$): δppm 7.05 (d, J = 8.6 Hz, 12H), 6.63 (d, J = 8.6 Hz, 12H). ^{13}C NMR (125 MHz, $C_2D_2Cl_4$): δppm 135.97, 135.09, 129.16, 126.90, 116.70. FD-MS(8 KV): 1007.3 (M^+), calcd. 1007.7. Elemental analysis: Calcd.: C50.04, H 2.40, Br 47.56; Found: C 50.06, H 2.40.

Hexakis(4-iodophenyl)hexaphenylbenzene(12). An 800-mg portion of compound **9** (0.56 mmol) was dissolved in 320 mL of degassed chloroform, to which 6.74 mL iodine monochloride (1.0 M in dichloromethane, 6.74 mmol) was added slowly via syringe. The mixture was stirred for 45 min, and then 100 mL of 10% aqueous sodium sulfite was added to quench the reaction. The organic layer was washed with water three times, dried over magnesium sulfate, and concentrated to 50 mL. Precipitation with 400 mL of methanol gave a white solid, which was dried under reduced pressure to give 900 mg of pure product (92%). mp > 410 °C. ^{1}H NMR (250 MHz, $C_2D_2Cl_4$): δ ppm 6.86 (d, J = 8.2 Hz, 12H), 7.04 (d, J = 8.2 Hz, 12H), 7.07 (d, J = 8.2 Hz, 12H), 7.57 (d, J = 8.2 Hz, 12H). ^{13}C NMR (125 MHz, $C_2D_2Cl_4$): δppm 142.63, 140.84, 138.91, 136.60, 135.19, 134.45, 130.86, 127.54, 124.05. FD-MS (8 KV): *m*/*z* 1746.8, calcd.1746.68. Elemental analysis: Calcd.: 53.64, H 2.77, I 43.59; Found: C53.65, H 2.77.

Hexakis(4-iodophenyl)hexabenzocoronene (5). A 500-mg portion of compound **12** (0.2862 mmol) was dissolved in 300 mL dichloromethane and 150 mL carbon disulfide, and the liquid was constantly sparged with argon. Then 4.64 g of anhydrous iron (III) chloride in 20 mL of nitromethane was added via syringe. After 1.5h reaction was quenched by 500 mL of methanol. The yellow precipitate was collected and washed by methanol until the filtrate was colorless, dried under reduced pressure to give 0.44 g insoluble product (90%). MALDI MS (TCNQ as matrix): 1734 (*m*/*z*). Elemental analysis: Calcd.: C 54.01, H 2.09, I 43.90; Found: C 53.87, H 2.10.

General Procedure for Sonogashira−Hagihara Coupling of Compound 5 and Monoethynylenes 13a−c. To a frame-dried 25 mL Shlenk flask, 300 mg compound **5** (0.173 mmol), 30 mg $Pd(PPh_3)_4$ (2.5 mol % per iodo), 10 mg of copper iodide (5.0 mol % per I), and 20 mL piperidine were added. The mixture was degassed by bubbling argon for 15 min, then 403 mg **13**a (2.076 mmol) was added. The solution was heated to 50 °C overnight, cooled to RT, and 20 mL methanol was added. The yellow precipitate was collected, followed by column chromatography (silica gel, PE/DCM = 3:2) to give 302 mg pure compound **14**a (82%). ^{1}H NMR (500 MHz, $C_2D_2Cl_4$, 413 K): δ ppm 0.93 (t, CH_3, 18H), 1.20−1.47 (m, −CH_2−, 96H), 1.68 (br, 12H), 1.87 (br, 12H), 2.65 (br, 12H), 7.43−7.56 (br, 24 H), 7.8−8.5 (br, 12H). ^{13}C NMR (125 MHz, CD_2Cl_2/CS_2 = 1:1): δ ppm 139.35, 132.55, 128.20, 126.94(m), 123.60, 121.85, 118.28(m), 92.01, 81.41, 32.79, 30.66, 30.60, 30.28 (m), 30.02, 23.64, 20.61, 14.85. MALDI MS (with TCNQ as matrix): *m*/*z* 2133, cal.2133.29. Elemental analysis: Calcd.: C 91.21, H 8.79; Found: C 91.16, H 8.74.

14b. CC: silica gel, DCM to DCM/THF = 4:1. 90.2%. ^{1}H NMR (500 MHz, $C_2D_2Cl_4$, 413 K): δ ppm 0.93 (br, CH_3, 18H), 1.35−1.51 (m, −CH_2−, 108H), 1.81 (br, 12H), 1.87 (br, 12H), 3.93 (br, 12H), 6.76 (br, H), 7.44 (br, 12H). ^{13}C NMR (125 MHz, CD_2Cl_2/CS_2 = 1:1): δ ppm 157.02, 136.61, 131.54, 129.70(m), 124.20(m), 120.41(m), 113.62(m), 112.49, 88.81, 86.92, 30.62, 28.42, 28.09, 24.78, 21.48, 12.70. MALDI MS (with TCNQ as matrix): *m*/*z* 2686, cal.2685.88. Elemental analysis: Calcd.: 88.54, H 7.88, O 3.57; Found: C 88.50, H 7.84.

14c. CC: silica gel, PE/DCM = 7:3, 77%. ^{1}H NMR (500 MHz, $C_2D_2Cl_4$, 413 K): δ ppm 0.88 (br, 54H), 1.31−1.51 (br, 324H), 1.81 (br, 36H), 4.02 (br, 36H), 6.84 (s, 12H), 7.86 (br, 12H), 8.04 (br, 12H), 9.26 (s, 12H). ^{13}C NMR (125 MHz, CD_2Cl_2/CS2 = 1:1): δ ppm 153.44, 140.95, 139.54, 138.07, 133.19, 130.25, 127.97, 123.96, 123.54, 120.52, 119.93, 117.62, 110.31, 91.95, 88.37, 69.37, 32.29, 30.77, 30.09, 29.76, 26.51, 23.06, 14.54. MALDI MS (with TCNQ as matrix): *m*/*z* 4898.03, cal.4897.77. Elemental analysis: Calcd.: C 83.87, H 10.25, O 5.88; C 83.85, H 10.26.

1-Bromo-3,4,5-tri(dodecyloxy) benzene (15). A 4.9-g portion of 1-bromo-(3,4,5-trimethoxy)benzene (20 mmol) was dissolved in 40 mL of dichloromethane, and the solution was cooled to −78 °C, followed by the slow addition of 60 mL BBr_3 (1 M in DCM). The mixture was allowed to warm to room temperature over 3 h and stirred for 28 h. The reaction was quenched by ice−water and the mixture was extracted with ethyl acetate (40 mL × 2). The organic layer was washed with water three times, dried over magnesium and concentrated under reduced pressure to 3.4 g 1-bromo-3,4,5-trihydoxybenzene as a white solid, which was directly submitted to the next reaction. 2.5 g of this solid was dissolved in 60 mL DMF and the solution was degassed by bubbling argon for 15 min, then 13.46 g K_2CO_3 (97.5 mmol) was added. The mixture was stirred at room temperature for 30 min, and then 13.61 g 1-bromododecane (54.6 mmol) was added. The mixture was heated to 60 °C for 4 h. After cooling, the mixture was poured into 100 mL ice−water and the white precipitate was collected, followed by column chromatography (silca gel, PE/DCM = 4:1) to afford 7.31 g pure product (85%) as white powder. mp 48.5 °C. ^{1}H NMR (250 MHz, CD_2Cl_2): δ ppm 0.86 (t, 9H), 1.25 (m, 48H), 1.40 (m, 6H), 1.76 (m, 6H), 3.8934 (m, 6H), 6.66 (s, 2H). ^{13}C NMR (125 MHz, CD_2Cl_2): δ ppm 14.26, 23.08, 26.43, 26.48, 29.66, 29.75, 30.01, 30.04, 30.08, 30.12, 32.32, 69.61, 73.71, 110.17, 115.74, 137.65, 154.25. FD-MS (8 KV): 710.9(M+), calcd. 709.98. Elemental analysis: Calcd.: C 71.05, H 10.93, Br 11.25, O 6.76; Found: C, 71.02, H 10.91.

1-Trimethylsilyl-3,4,5-tri(dodecoxyphenyl)acetylene (16). To a 50-mL two-neck flask, 2.5 g compound **15** (3.52 mmol), 517 mg $Pd(PPh_3)_4$ (2 mol %), 33.6 mg of copper (I) iodide (5 mol %) and 10 mL piperidine were added. The mixture was degassed by two "freeze−pump−thaw" cycles, then 517 mg of trimethylsilylacetylene (5.26 mmol) was added and the whole heated to reflux overnight. After cooling, the reaction was quenched with 20 mL 2 M aqueous ammonium chloride. The mixture was extracted with diethyl ether (30 mL × 3), and the organic layer washed with water three times, dried over magnesium sulfate, concentrated under reduced pressure, and the residue was purified by column chromatography (silica gel, PE/DCM = 4:1) to give 4.2 g title product (92.5%). ^{1}H NMR (250 MHz, CD_2Cl_2): δ ppm 0.23 (s, 9H), 0.88 (t, 9H), 1.27 (m, 48H), 1.41(m, 6H), 1.75 (m, 6H), 3.92 (m, 6H), 6.64(s, 2H). ^{13}C NMR (125 MHz, CD_2Cl_2): δ ppm 0.04,14.27, 23.10, 26.48, 29.77, 29.79, 29.98, 30.04, 30.10, 30.13, 30.70, 32.34, 69.45, 73.78, 92.80, 105.75, 110.44, 117.82, 139.54, 153.34. FD-MS: 727.31, calcd.: 727.29 (M^+). Elemental analysis: Cal.: C77.62, H 11.92, O 6.60, Si 3.86; Found: C 77.58, H11.94.

3,4,5-Tri(dodecyloxy) phenylacetylene (13c). 1.2 g compound **16** (1.65 mmol) was dissolved in 8 mL dichloromethane and 8 mL of methanol, and then 683.1 mg potassium carbonate (4.95 mmol) was added. The mixture was stirred for 3 h at room temperature and extracted with 50 mL DCM. The organic layer was washed with water, dried over magnesium sulfate, concentrated under reduced pressure and the residue was purified by column chromatography (silica gel, PE/DCM = 4:1) to give 1.03 g title product (96%). mp 49.2 °C. ^{1}H NMR (250 MHz, CD_2Cl_2): δ 0.88 (t, 9H), 1.27 (m, 48H), 1.41 (m, 6H), 1.75 (m, 6H), 3.04 (m, 6H), 3.92 (m, 6H), 6.68 (s, 2H). ^{13}C NMR (125 MHz, CD_2Cl_2): δ 14.66, 23.48, 26.88, 30.11, 30.16, 30.36, 30.42, 30.44, 30.48, 30.51, 31.08, 32.72, 69.84, 74.19, 76.36, 84.64, 111.10, 117.08, 153.77. FD-MS: 655.12, calcd.: 655.11(M^+). Elemental analysis: Calcd.: C 80.67, H 12.00, O 7.33; Found: C 80.64, H 11.96.

Acknowledgment. This work was financially supported by the Zentrum für Multifunktionelle Werkstoffe und Miniaturisierte Funktionseinheiten (BMBF 03N 6500), EU-TMR project SISITOMAS, the Deutsche Forschungsgemeinschaft (Schwerpunkt Feldeffekttransistoren), and the EU project DISCEL (G5RD-CT-2000-00321).

Supporting Information Available: MALDI MS and temperature-dependent ^{1}H NMR characterization of **14a**−**c**, DSC curves, powder and 2D X-ray diffraction results for **14a**−**c** and selected AFM images for **14b** and **14c**. This material is available free of charge via the Internet at http://pubs.acs.org.

JA037519Q